Journal of The Electrochemical Society

Thermal Runaway Propagation in Li-ion Battery Packs Due to Combustion of Vent Gases

To cite this article: Dhananjay Mishra *et al* 2022 *J. Electrochem. Soc.* **169** 100520

View the article online for updates and enhancements.

This content was downloaded from IP address 129.107.89.228 on 04/11/2022 at 17:03

Journal of The Electrochemical Society, 2022 **169** 100520
1945-7111/2022/169(10)/100520/10/$40.00 © 2022 The Electrochemical Society ("ECS"). Published on behalf of ECS by IOP Publishing Limited

Thermal Runaway Propagation in Li-ion Battery Packs Due to Combustion of Vent Gases

Dhananjay Mishra,[1] Peng Zhao,[2] and Ankur Jain[1,z]

[1]*Mechanical and Aerospace Engineering Department, University of Texas at Arlington, Arlington, Texas, United States of America*
[2]*Department of Mechanical, Aerospace & Biomedical Engineering, UT Space Institute, University of Tennessee - Knoxville, United States of America*

Accurate understanding of propagation of thermal runaway is of much importance for developing safe battery pack designs. Combustion of vent gases emerging from a trigger cell undergoing thermal runaway has not been studied in sufficient detail, even though the additional heat generated during combustion likely plays an important role in thermal runaway propagation. This work presents comprehensive numerical modeling and simulations of thermal runaway propagation in a pack of cylindrical cells. The model accounts for multiple coupled non-linear phenomena, including vent gas flow and combustion, radiation and thermal runaway. Non-premixed combustion of venting gas is modeled using k-ε turbulence model and finite rate chemical kinetics. Simulation results are shown to be in good agreement with experimental data for a benchmark turbulent non-premixed jet flame. Simulations show that hot combustion products are rapidly transported in gaps between cells, potentially leading to self-sustained thermal runaway propagation to adjacent cells. Results demonstrate the critical importance of combustion in determining the nature of propagation of thermal runaway. The vent hole location is identified as an important parameter that influences whether and the extent to which thermal runaway propagation occurs. This work contributes towards the practical understanding of thermal runaway safety of Li-ion battery packs.
© 2022 The Electrochemical Society ("ECS"). Published on behalf of ECS by IOP Publishing Limited. [DOI: 10.1149/1945-7111/ac91a7]

Manuscript submitted June 16, 2022; revised manuscript received August 16, 2022. Published October 18, 2022.

Thermal runaway in Li-ion cells is a well-known and widely researched phenomenon that directly impacts the safety, reliability and performance of electrochemical energy storage and conversion devices.[1,2] The onset of thermal runaway occurs when overheating of the cell results in initiation of exothermic reactions, leading to even greater heat generation. Due to the non-linear Arrhenius nature of heat generation, this results in a positive feedback loop, which, if not prevented, may result in destruction of the cell and subsequent fire. Such exothermic reactions underlying thermal runaway include decomposition of the solid-electrolyte-interphase (SEI) layer, electrode-electrolyte reaction and electrolyte decomposition.[3] Semi-global Arrhenius parameters for these processes for various cell chemistries have been acquired through thermal calorimetry experiments and have been widely used in theoretical and simulation studies.[3,4] Thermal runaway is triggered by the competition between chemical heat release and heat loss, and is, in principle, similar to any thermal ignition process. After thermal runaway is triggered, rupture of the cell body often occurs, resulting in venting of hot gases and particles.[5] These venting substances are often hydrocarbon-dominant, and therefore, can trigger combustion and fire with suitable mixture composition and temperature, thus potentially contributing towards thermal runaway propagation.

Propagation of thermal runaway from one cell to another is a very important problem from a system-level safety perspective. While thermal runaway limited to a single cell is undesirable but potentially manageable, on the other hand, propagation to neighboring cells, then further to their neighbors and so on results in destruction of the entire battery pack and a widespread fire at a much larger scale. Therefore, understanding the nature of thermal runaway propagation and the parameters that affect this process is of paramount importance. Accordingly, a number of experimental and computational studies in this direction have been reported.[6] Thermal runaway characteristics for $LiFePO_4$, $Li(Ni_{0.45}Mn_{0.45}Co_{0.10})O_2$ and combination of $LiCoO_2$ and $Li(Ni_{0.5}Mn_{0.25}Co_{0.25})O_2$ chemistries has been studied.[7] For $Li(Ni_xCo_yMn_z)O_2$ type cathode cell, redox reaction between cathode and carbon based anode at high temperatures was identified as the major heat source.[8] The influence of ageing on thermal runaway has been investigated.[9] Several studies have investigated mitigation of cascade failure following thermal runaway onset in one of the cells in a battery pack. Measurements on arrays of 18650 cells have shown greater thermal runaway propagation speed in air than in nitrogen.[10] Thermal runaway propagation in a battery pack for different module configurations has been studied using heat-to-vent setting for a single cell.[11] The impact of heating power and heating area on thermal runaway onset has been studied.[12] The impact of SOC[13] and battery chemistry[14] on thermal runaway propagation has been studied experimentally. Measurements on cylindrical and pouch cells have indicated the important role of high electrical conductivity shell and large contact surface area on thermal runaway propagation.[15] While experiments provide useful insights into realistic scenarios, simulations-based investigations are equally important due to the cost and complexity of measurements. Analytical[16–18] and numerical models[19,20] to predict thermal runaway have been studied, with the goal to predict, delay or prevent thermal runaway propagation. The importance of thermal properties of the interstitial material between cells in a battery pack has been recognized, and it has been shown that an intermediate thermal conductivity results in an optimum balance between the risks of thermal runaway initiation and thermal runaway propagation.[21] The importance of radiative heat transfer has been recognized[22] and the use of radiative shields for heat removal and thermal runaway prevention has been investigated.[23] Prediction of thermal runaway propagation as a probabilistic event has been investigated.[24]

The flow of vent gases following rupture of a failed cell is an important event in thermal runaway, as high speed flow of extremely hot vent gases may spread heat to neighboring cells even in presence of thermal insulation between cells. Moreover, combustion of the volatile vent gases may further contribute towards thermal runaway propagation. Experimentally validated lumped models for single cell have been used to characterize thermal runaway onset during venting in a single cell.[25,26] A mathematical model for predicting temperature-pressure dependence and gas generation within 18650 cell has been developed.[5] The impact of vent gas flow on thermal runaway propagation in battery pack has been studied through simulations.[27] Evolution of temperature and pressure within the cell during thermal runaway and vent gas combustion has been studied through computational fluid dynamics (CFD) simulations.[28]

Kinetic mechanisms, gas generation and venting, and subsequent fire and thermal runaway propagation have been studied extensively. Heat of combustion has been measured as a function of SOC using fire propagation apparatus for commercial pouch cells.[29]

[z]E-mail: jaina@uta.edu

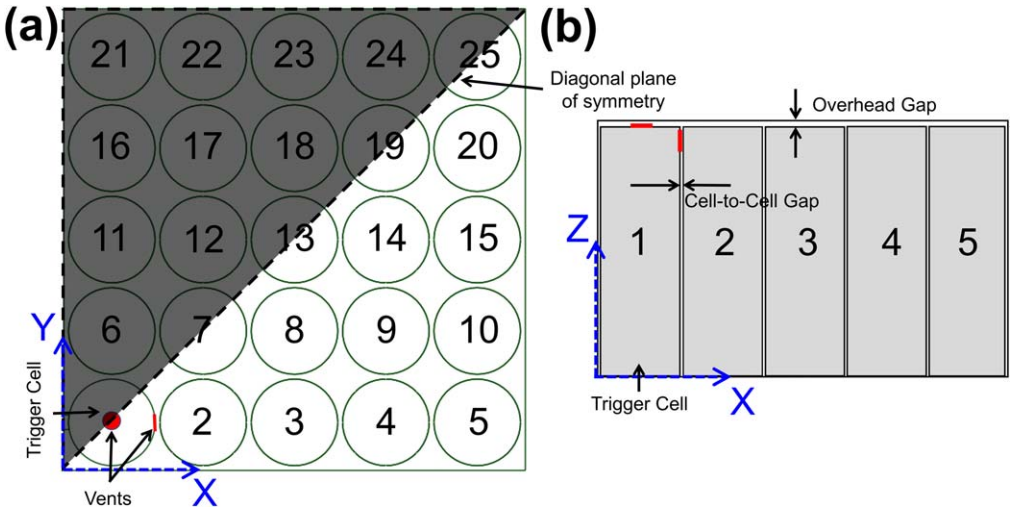

Figure 1. (a) Schematic of the simulation geometry for a 5 by 5 Li-ion battery pack. The half-geometry modeled in this work based on symmetry is indicated; (b) Cross-section view of the geometry in the XZ plane. Cell 1 is the trigger cell, with the vent hole located either at the top end or on the curved surface, as shown.

Dependence of heat release rate and toxic gas emissions on SOC has also been reported using short circuit, propane fire test and external heating test.[30] Investigations on fire induced toxicity for Li-ion cells using Tewarson calorimeter have highlighted the role of anion salt in dictating toxicity.[31,32] Mitigation techniques for Li-ion battery fire suppression using water mist with CO_2 and HFC-227EA,[33] and water and $C_6F_{12}O$[34] have been studied. Effect of arrangement of cells in the pack on fire behavior for $LiCoO_2$ 18650 cells has been studied using heat flux, mass flowrate and heat release rate measurements.[35] Experimentally validated analytical models[36] for 21700 NMC cells and 3D heat simulation model[37] for 18650 cells for battery fire characterization have been presented.

Despite the literature cited above, several challenges in the modeling of combustion during thermal runaway remain. For example, thermal runaway kinetic mechanisms frequently involve semi-global reactions, for which, there is a lack of understanding and quantification of elementary reaction pathways. Further, while experimental measurements of vent gas generation have been reported, such measurements are frequently global instead of local, and integrated instead of *in situ*. Finally, without reliable venting gas models, the modeling of subsequent venting fire and thermal runaway propagation is frequently decoupled with vent gas generation. As a result, the important interaction between venting fire and venting gas generation is not effectively modeled. In general, numerical simulation of thermal runaway in a battery pack is computationally challenging due to the non-linear nature of several processes involved in thermal runaway. Around the time of thermal runaway initiation, heat generation rate increases very rapidly with temperature, and, therefore, an extremely small timestep is needed to properly resolve the problem. In addition, radiative heat transfer is also a non-linear transport process. Such challenges are exacerbated with the inclusion of venting gas combustion, which not only provides non-linear thermal feedback to the upstream thermal runaway initiation, but also affects flow and heat transfer downstream, leading to thermal runaway propagation. In general, radiation and combustion are both important heat transfer related processes during thermal runaway propagation, and must be considered together in order to rigorously evaluate thermal runaway. Despite such challenges, development of robust numerical simulation tools continues to be very important, because such simulations can help design thermal runaway experiments, and contribute towards optimized battery packs for reduced risk of thermal runaway propagation.

This work presents numerical simulation of the onset and propagation of thermal runaway in a Li-ion battery pack, with specific emphasis on investigation of the effects of combustion of vent gases. All three modes of heat transfer - conduction, convection and radiation - are accounted for. Arrhenius heat generation due to four decomposition reactions is modeled. The non-premixed combustion of venting gas is modeled using the standard k-ϵ model for turbulence and finite rate detailed chemical kinetics. Following validation of the numerical simulation framework by comparison with a benchmark experimental data, the simulation is used for understanding the impact of the combustion process on propagation of thermal runaway from the trigger cell to its neighbors.

The next section presents describes the simulation setup, including the governing physics modeled in the simulations, geometry of the battery pack and computational details. Key results, including validation and parametric analysis are presented in the subsequent section, followed by concluding remarks.

Simulation Model

Geometry.—The geometry considered here comprises a 5 by 5 matrix of cylindrical 18650 cells in a cuboidal box, as shown schematically in Fig. 1a. Wherever possible, only the unshaded right half of the geometry shown in Fig. 1a is simulated by taking advantage of symmetry. As a baseline case, bottom left cell is taken to be the trigger cell that undergoes thermal runaway first. High speed flow and combustion of hot vent gases emerging from a vent hole on the trigger cell is of particular interest in the present work. Key geometrical parameters here include cell-to-cell gap, overhead gap and position of vent on the trigger cell, as shown in the XZ plane cross-section in Fig. 1b. The area of the circular vent is taken to be 7 mm^2, based on past measurements of the vent opening area in a specific thermal runaway measurement.[38] In order to investigate the effects of various geometrical and other parameters, two distinct positions of the vent hole are considered. The first one is at the center of the top surface of the trigger cell, which may represent opening of the pressure vent or outright failure of the top cap of the cell. The second is located at 62.5 mm height on the curved surface of the cell pointing towards cell 2, which may represent failure of the cell body due to pressure accumulation within the cell during thermal runaway. The entire battery pack is placed inside a cuboidal box. Due to complexity of simulation and extensive computational requirements, venting is only considered from the trigger cell. Also, these simulations model a battery storage scenario, and therefore, charging/discharging of cells is neglected.

Finite-volume heat transfer and fluid flow simulations are carried out in ANSYS Fluent to account for heat generation due to combustion of hot ejecta flowing out at high velocity from the trigger cell. Radiative heat transfer between cells is modeled using surface-to-surface radiation method. Thermal runaway propagation due to thermal abuse and temperature-dependent heat generation in each cell is modeled using Arrhenius chemistry. The next subsection describes the governing equations for each of these phenomena that are solved in order to investigate the propagation of thermal runaway in these conditions.

Governing equations.— *Non-premixed combustion transport equations.*—Non-premixed combustion model relates the instantaneous thermochemical state of a species to mixture fraction, which is modeled as a conserved scalar quantity.[39] This combustion modeling approach, therefore, involves solving the mixture fraction transport equations, and not the individual species equations. The mixture fraction is defined as:

$$\mathrm{f} = \frac{\mathrm{Z_i} - \mathrm{Z_{i,ox}}}{\mathrm{Z_{i,fuel}} - \mathrm{Z_{i,ox}}} \quad [1]$$

Where $\mathrm{Z_i}$ is the mass fraction for element i. Subscripts *ox* and *fuel* represent the oxidizer and fuel, respectively. Due to very high vent speed, flow is assumed to be turbulent, based on which, the assumption of equal diffusivities for individual species is reasonable, since turbulent convection generally overwhelms molecular diffusion. Following this assumption, transport equation for the density averaged mixture fraction f′ may be written as

$$\frac{\partial(\rho \mathrm{f}')}{\partial \mathrm{t}} + \nabla\cdot(\rho \mathrm{uf}') = \nabla\cdot\left(\left(\frac{k}{C_p} + \frac{\nu_t}{\mathrm{Pr}}\right)\nabla \mathrm{f}'\right) + S_m \quad [2]$$

where k, C_p, and Pr are mixture thermal conductivity, specific heat and Prandtl number, respectively. S_m is the rate of transfer of mass from the fuel to the gas phase.

In addition, the conservation equation for mass fraction variance is given by

$$\frac{\partial(\rho f''^2)}{\partial \mathrm{t}} + \nabla\cdot(\rho \mathrm{uf}''^2) = \nabla\cdot\left(\left(\frac{k}{C_p} + \frac{\nu_t}{\mu_t}\right)\nabla \mathrm{f}''^2\right) + C_g \nu_t (\nabla \mathrm{f}')^2 - C_d \rho \frac{\varepsilon}{k} f''^2 \quad [3]$$

f''^2 is the mixture fraction variance, with $\mathrm{f}'' = \mathrm{f} - \mathrm{f}'$. Values for constants C_g, C_d are 2.86 and 2.0 respectively. Thermal diffusivity for the turbulent flow is considered equal to the mass diffusivity.

Mass fraction, density and temperature are assumed to be functions of the mixture fraction. In this case, heat gain/loss is parameterized as follows

$$\Phi_\mathrm{i} = \Phi_i(\mathrm{f}', \mathrm{H}) \quad [4]$$

where Φ_i represents mass fraction, density or temperature and H represents the instantaneous enthalpy. Mean scalars for each species are calculated as:

$$\Phi_i' = \int_0^1 \Phi_i(\mathrm{f}', \mathrm{H})\mathrm{p}(\mathrm{f}')\mathrm{df}' \quad [5]$$

where $\mathrm{p}(\mathrm{f}')$ is a probability density function. Finally, energy equation for the non-premixed combustion model is written in the mean enthalpy form as follows:

$$\frac{\partial[\rho \mathrm{H}]}{\partial \mathrm{t}} + \nabla\cdot[\rho \mathrm{uH}] = \nabla\cdot\left[\frac{k_{eff}}{C_p}\nabla \mathrm{H}\right] + S_h \quad [6]$$

Here, species diffusion and conduction collectively contribute towards the first term on the right-hand side. Equation 6 is written in terms of the total enthalpy H. Total enthalpy of individual species is defined as:

$$\mathrm{H_i} = \int_{\mathrm{T_{ref,i}}}^{\mathrm{T}} \mathrm{C_{p,i}dT} + \mathrm{h_i^0[T_{ref,i}]} \quad [7]$$

Where, $\mathrm{h_i^0[T_{ref,i}]}$ is the enthalpy of formation of species i and $\mathrm{T_{ref,i}}$ is the reference temperature. Combustion model is described by finite rate chemistry, where a reduced C_2H_4 combustion model including 32 species and 206 elementary reactions simulates the venting flame. This model has been extensively validated against C0-C2 combustion targets.[40]

Mass, momentum and energy transport equations.—High speed flow of ejecta combined with combustion presents stability challenges in numerical computation. As a result, the k-ε model is used,[41] which offers high numerical stability without the need for damping functions. This turbulent flow model comprises two equations, which solve for turbulent kinetic energy and specific dissipation rate. This model also accounts for the effects of stream turbulence and mass injection. The mass conservation equation is written as:

$$\nabla\cdot(\rho \mathbf{V}) = 0 \quad [8]$$

The transport equations for turbulent kinetic energy (E_t) and specific dissipation rate (ε) are given by:

$$\frac{\partial(\rho E_t)}{\partial \mathrm{t}} + \nabla\cdot(\rho E_t u) = \nabla\cdot\left[\left(\mu + \frac{\mu_t}{Pr_k}\right)\nabla E_t\right] + \mathrm{G_k} + \mathrm{G}_b - \mathrm{Y_m} + \mathrm{S_k} - \rho\varepsilon \quad [9]$$

$$\frac{\partial(\rho\varepsilon)}{\partial \mathrm{t}} + \nabla\cdot(\rho\varepsilon u) = \nabla\cdot\left[\left(\mu + \frac{\mu_t}{Pr_\varepsilon}\right)\nabla\varepsilon\right] + C_{1\varepsilon}\frac{\varepsilon}{E_t}[G_k + C_{3\varepsilon}G_b] - C_{2\varepsilon}\frac{\rho\varepsilon^2}{E_t} + S_\varepsilon \quad [10]$$

Here, G_k represents the generation of turbulence kinetic energy due to mean velocity gradients, G_b is the generation turbulent kinetic energy due to buoyancy and Y_m represents fluctuating dilatation in compressible turbulence to overall dissipation rate. Pr_k and Pr_ε represent turbulent Prandtl numbers for kinetic energy and dissipation rate, respectively. S_k and S_ε denote user defined source terms. $C_{1\varepsilon}$, $C_{2\varepsilon}$, Pr_k and Pr_ε are constants with experimentally determined values of 1.44, 1.92, 1.0 and 1.3 respectively.

Similarly, turbulent heat transport equation for the turbulent flow can be written as

$$\frac{\partial(\rho \mathrm{E})}{\partial \mathrm{t}} + \nabla\cdot[u\,(\rho \mathrm{E} + \mathrm{p})] = \nabla\cdot\left[\left(\mathrm{k} + \frac{\mathrm{C_p}\mu}{Pr}\right)\nabla \mathrm{T} + u\cdot\bar{\bar{\tau}}\right] + \mathrm{S_{hs}} \quad [11]$$

where k is the effective thermal conductivity, E is total energy, S_{hs} is the heat source term and $\bar{\bar{\tau}}$ is a deviatoric stress tensor.

Thermal conduction.—Heat transfer within each solid cell is governed by the three-dimensional thermal conduction equation in cylindrical coordinates, given by

$$\frac{\mathrm{k_r}}{\mathrm{r}}\frac{\partial}{\partial \mathrm{r}}\left(\mathrm{r}\frac{\partial \mathrm{T}}{\partial \mathrm{r}}\right) + \frac{\mathrm{k}_\theta}{\mathrm{r}^2}\frac{\partial^2 \mathrm{T}}{\partial \theta^2} + \mathrm{k_z}\frac{\partial^2 \mathrm{T}}{\partial \mathrm{z}^2} + \mathrm{q}''' = \rho \mathrm{c_p}\frac{\partial \mathrm{T}}{\partial \mathrm{t}} \quad [12]$$

where thermal conductivity within the cell is taken to be homogeneous and cylindrically orthotropic. All properties are assumed to

be independent of temperature. In Eq. 12, q''' represents volumetric heat generation within the cell due to decomposition reactions, as discussed in more detail next. Radial, axial and circumferential thermal conductivities of 0.2, 32 and 32 $Wm^{-1}K^{-1}$, density of 2280 kgm^{-3} and heat capacity of 715 $Jkg^{-1}K^{-1}$ are assumed, based on past work.[18,42]

Heat generation.—Heat is generated within each cell due to decomposition reactions, including SEI decomposition, negative solvent reaction, positive solvent reaction and electrolyte decomposition reactions respectively. Arrhenius-based reaction parameters for these standard set of equations corresponding to $LiCoO_2$ cell chemistry are used. The governing equations and values of reaction parameters are readily available in past work.[27]

Radiative heat transfer.—Radiative heat transfer between surfaces of cells is explicitly modeled based on surface-to-surface radiative heat exchange. View factors are calculated using the ray tracing method. Details of the radiation model, including validation are described in a past paper.[21]

Isentropic flow equations.—Temperature and velocity distribution of the hot ejecta from the vent hole are determined as functions of time using isentropic flow equations. These equations are based on mass flow rate and stagnation pressure measurements from previous experimental work.[38] Thermophysical properties of the ejecta are calculated using weighted average using an open source software.[43] The individual gaseous species (CO_2, H_2, C_2H_4, CO, CH_4, C_2H_6) correspond to LCO type cathode 18650 cells.[44] The ejecta originating from trigger cell is assumed to contain 17.5% H_2, 33.8% CO_2, 39.9% CO, 5.2% CH_4, 3.2% C_2H_4 and 0.4% C_2H_6 by mole respectively. The hot ejecta leaving the trigger cell is treated to be a calorically perfect gas. The equations derived based on stagnation flow analysis establish direct relationship between stagnation pressure and Mach number, and an inverse relationship between venting temperature and stagnation pressure. The inverse relationship between temperature and velocity of the ejecta signifies the conversion of pressure energy into intermolecular energy. More details on isentropic flow calculations are available in a past paper.[27]

Meshing and other simulation details.—Appropriate discretization of the simulation domain is critical for obtaining good convergence, particularly in the present case that combines multiple non-linear processes. All simulations in this work use 3D polyhedral mesh due to low numerical diffusivity and semi-automatic generation. These characteristics not only result in better approximation of gradients across the elements, but also offer better mesh resolution in complex geometries. Polyhedral elements are less sensitive to stretching, which results in improved numerical stability and more accurate solution with lower cell count as compared to other types of meshing elements. In these simulations, upwards of 10.1 million elements are used with a growth rate of 1.05, squish index of 0.38 and orthogonal quality of 0.67.

Temperature and pressure boundary conditions for the vent are obtained using isentropic flow analysis, as described in previous work.[27] While the vent temperature increases monotonically with time, vent velocity rises, reaches a peak, and then reduces as the cell runs out of vent gas to eject. Natural convective cooling boundary condition is used for all surfaces of the battery pack except the diagonal symmetry plane shown in Fig. 1a, which is modeled as an adiabatic surface. Except the vent hole, flow boundary conditions on the outer surfaces as well as cell surfaces include no slip and no normal flow.

Combustion and supersonic flow of ejecta around cells results in tremendous heat release in a very short span of time. These peculiar characteristics escalate the non-convergent behavior of energy equation, requiring very small time steps, especially close to thermal runaway. This is addressed by using a 10 μs constant time stepping with 10^{-4} relative tolerance. As described in the next section, a comprehensive time step sensitivity analysis is performed, and time step is determined based on the tradeoff between numerical accuracy and efficiency.

Results and Discussion

Time-step and mesh sensitivity analysis.—It is important to establish independence of simulation results from the timestep and mesh size in order to ensure accuracy. Towards this, a representative problem is simulated for different values of the timestep and for different number of elements in spatial discretization. In this case, LCO chemistry is assumed for each cell with a 2 s venting time. Overhead gap and cell-to-cell gap are 1 mm and 4 mm, respectively. The vent hole size is 7 mm^2, located at the top surface of the trigger cell. For these conditions, Fig. 2a plots maximum surface temperature on cell 2 as a function of time for different values of the time step. Even with a relatively small timestep of 50 μs, Fig. 2a shows that there is significant noise in the predicted temperature profile. A timestep of 10 μs or lower is needed for reasonable convergence in the temperature profile, so that there is no significant change in the temperature field with further reduction in the timestep. The very small timestep needed for convergence is a significant computational burden and is likely due to the severely non-linear nature of several aspects of this problem, including Arrhenius heat generation and radiation.

Similar to timestep sensitivity, the influence of spatial discretization on the computed temperature profile is investigated in Fig. 2b. These data show that the temperature field converges only with around 10 million or greater number of elements. Similar to the small timestep needed, this is also a significant computational burden, but is necessary to ensure accuracy.

In light of the results in Fig. 2, all subsequent simulations presented in this work are carried out with 12.5 million elements and with a timestep of 1 μs.

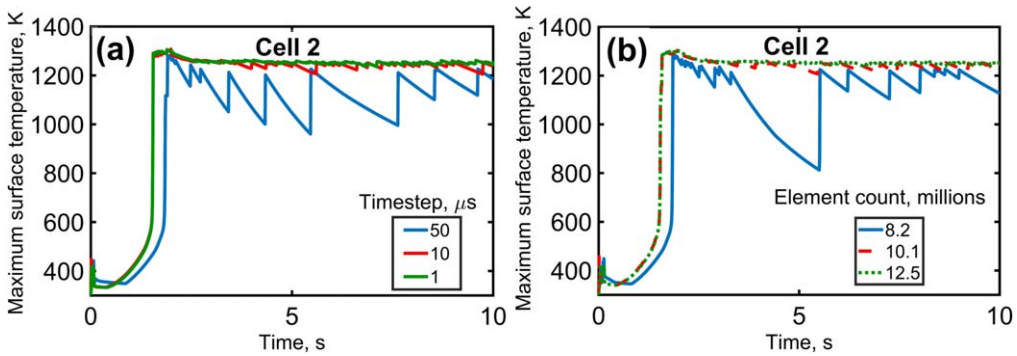

Figure 2. Simulation results to establish time step sensitivity and grid independence: Maximum surface temperature on cell 2 as a function of time for (a) different time steps, and (b) different mesh sizes. Problem parameters include 1 mm overhead gap, 4 mm cell-to-cell gap, 2 s venting time, LCO cathode and 7 mm^2 vent placed at center of top surface of cell 1. In (a), the element count is 12.5 million, and in (b), the timestep is 1 μs.

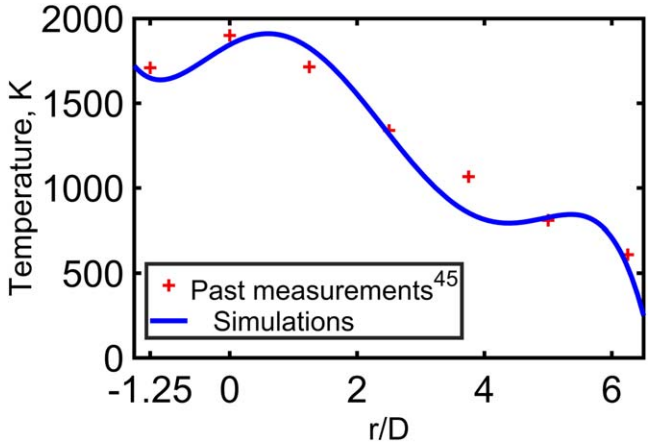

Figure 3. Validation plots for the combustion model: Radial variation in temperature at 40 mm distance from a nozzle for Raman/Rayleigh combustion process. Numerical simulation results are compared with past experimental data.[45] Fuel molar composition is 22.1% CH_4, 33.2% H_2, 44.7% N_2. Other simulation parameters include 42.2 ms^{-1} jet velocity, Reynolds number of 15200 and 8 mm nozzle diameter.

Validation of simulation model.—Due to the considerable complexity of the simulation model described in the previous section, including multiple coupled and non-linear phenomena, it is important to carry out a robust validation of the simulation model. This is done by comparison with classical Raman/Rayleigh/LIF measurements in a benchmark turbulent $CH_4/H_2/N_2$ jet diffusion flame.[45] These measurements have been reported for combustion of a fuel exiting from an 8 mm diameter nozzle. The fuel used for combustion consists of 22.1% methane, 33.2% hydrogen and 44.7% nitrogen by mole. The average flow velocity of the fuel is 42.2 m s^{-1} and the Reynolds number is $Re = 15200$. The stoichiometric mixture fraction is 0.167 and the flame adiabatic temperature is 2130 K. These experimental data have been widely used in the past for verification of detailed chemistry, flow and transport modeling in reacting flows.[46,47] For the present work, measurements of temperature and mass fraction of combustion products reported in the past are used for validation of the simulation model.

The simulation model is computed for the same set of conditions as the experiments. Comparison between the two is carried out in terms of radial distribution of temperature, as shown in Fig. 3, and H_2O and CO_2 concentrations, as shown in Figs. 4a and 4b, respectively, at a 40 mm distance from the nozzle tip. These plots show very good agreement between simulations and experimental data[45] for both temperature and species concentration. The thermal and chemical structures of the non-premixed flame reflect the dominant physical-chemical processes of chemical kinetics, molecular and turbulent diffusion. This validation exercise provides good confidence in the combustion modeling utilized in this work.

Combustion process during thermal runaway.—In order to further investigate the combustion phenomenon and to ensure that the simulation correctly captures the combustion process, distributions of key combustion products as well as the temperature distribution are examined as functions of time. Figures 5a and 5b present contours of the concentration distribution of H_2O and OH radicals, respectively, on the XY plane above the top end of cells at multiple times Fig. 6 presents similar temperature profiles. H_2O is a major product of the combustion process, and the OH radical is a good indicator of the reaction front location. At early times, say, $t = 0.001$ s, the peak of H_2O and OH in Fig. 5 and the temperature profile in Fig. 6 all indicate a regular flame structure with a thin reaction zone. Due to the very large vent velocity, venting gas, fresh air entrainment and hot combustion products quickly mix with each other and form a partially premixed reacting mixture. As time passes, the reaction region becomes much thicker and starts propagating into the rest of the domain, as seen in the plots at $t = 0.01$ s, when the venting flame has spread to nearly two-thirds of the domain along the X direction. Within 0.1 s, the high temperature region has already occupied near half of the XY plane, leading to exposure to high temperature (greater than 1000 K) for the rest of cells.

Impact of combustion on thermal runaway propagation.—In order to characterize the impact of combustion on the propagation of thermal runaway, two sets of simulations are carried out for a nominal set of conditions. The vent gas is assumed to eject from a 7 mm^2 hole at the center of top surface of the trigger cell. The vent duration is 2 s, and the overhead and cell-to-cell gap are 5 mm and 4 mm, respectively. In the first case, combustion of the venting gases is modeled, whereas, in the second case, the gases are assumed to vent out of the cell but not undergo combustion. For these two cases, Figs. 7a and 7b plot maximum temperatures in various cells in the battery pack as functions of time. It is seen clearly from Fig. 7b that when only venting is modeled, several cells, such as cells 2, 3 and 4 attain high temperature, but the thermal runaway is not sustained in any neighboring cell. At the end of the venting event, i.e., $t = 2$ s, all cells start to cool down. Eventually, there is no propagation of thermal runaway from the trigger cell into any other cells. On the other hand, as shown in Fig. 7a, when the combustion of the venting gases is correctly modeled, the additional heat generated due to combustion is sufficient to cause thermal runaway to propagate into cell 2, as characterized by sustained high temperature on cell 2.

Note that these Figures plot the maximum temperature that occurs on the cell surface, and not the temperature at a specific location. This is done because it is the maximum temperature that governs the occurrence of thermal runaway, and not necessarily the temperature at a specific location. It is found that the peak

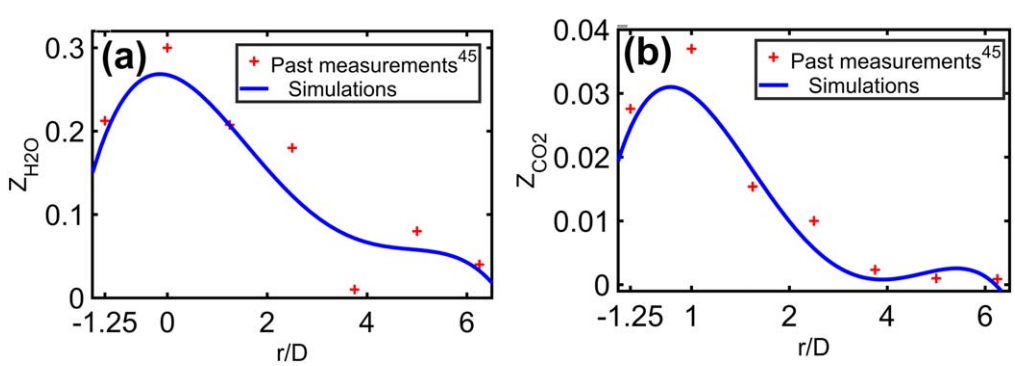

Figure 4. Validation plots for the combustion model: Radial variation in mass fraction for (a) water and (b) carbon dioxide at 40 mm distance from nozzle for Raman/Rayleigh combustion process. Numerical simulation results are compared with past experimental data.[45] Fuel molar composition is 22.1% CH_4, 33.2% H_2, 44.7% N_2 composition. Other simulation parameters include 42.2 ms^{-1} jet velocity, Reynolds number of 15200 and 8 mm nozzle diameter.

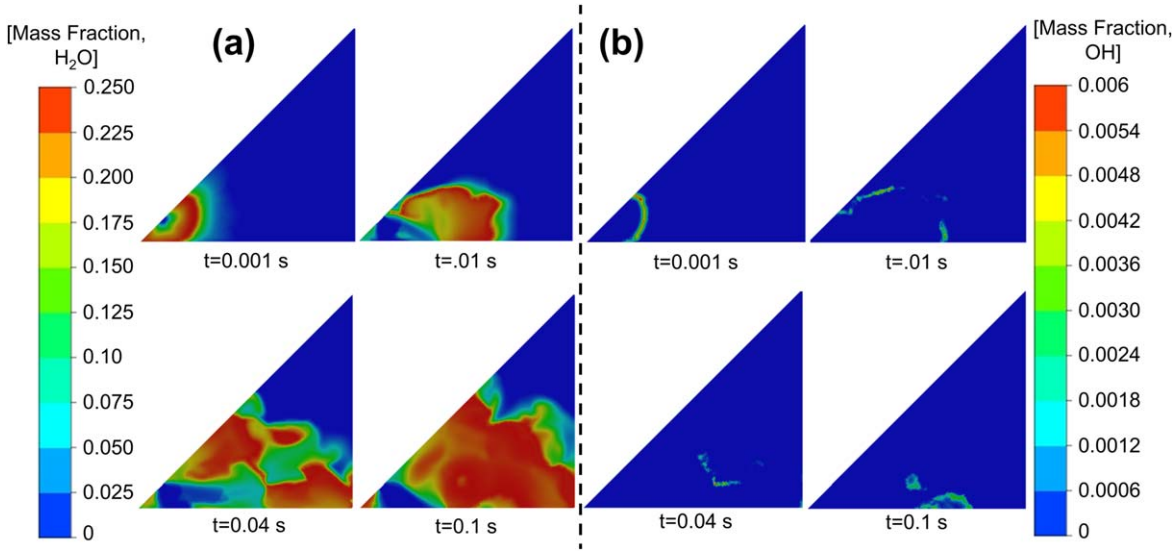

Figure 5. Color plots showing (a) H_2O and (b) OH radical concentrations at multiple times on an XY cross-section plane 1 mm above the top end of cells. Problem parameters correspond to Fig. 2.

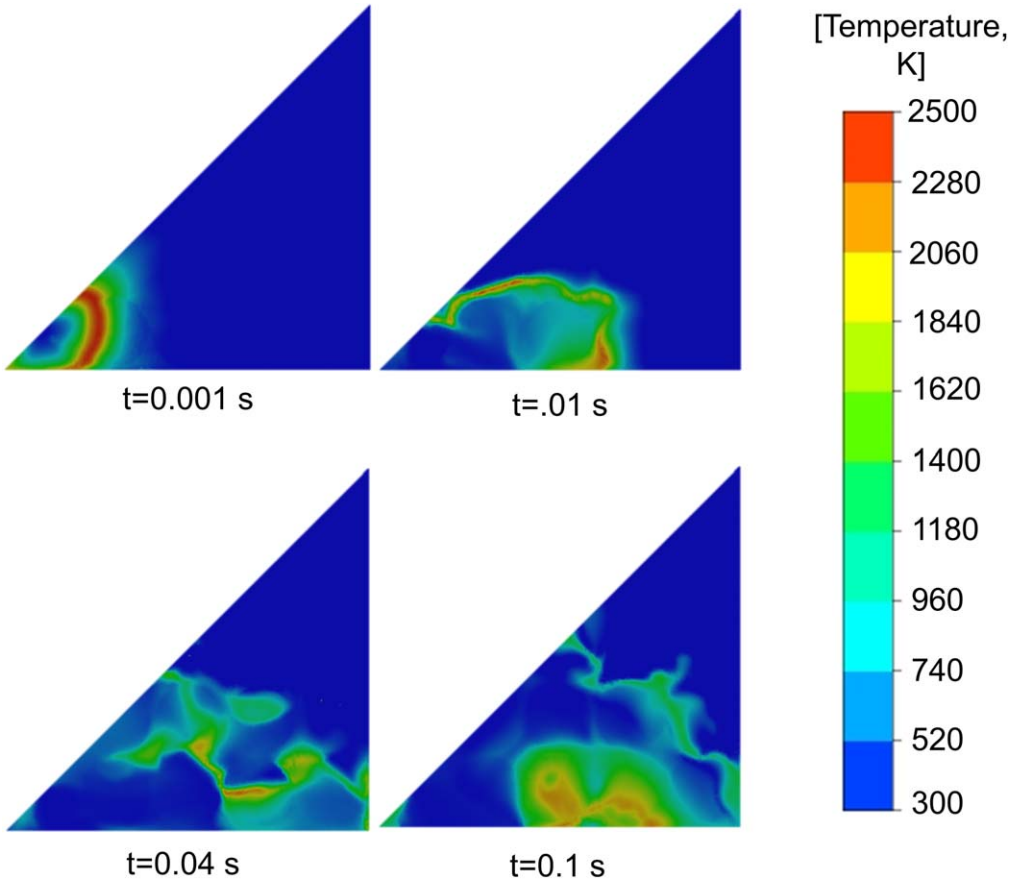

Figure 6. Color plots showing temperature distribution at multiple times on an XY cross-section plane 1 mm above the top end of cells. Problem parameters correspond to Fig. 4.

temperature typically occurs on or close to the top surface of the cells, consistent with the ejection of hot vent gases from and combustion very close to the top surface.

These results clearly indicate the importance of the combustion process during thermal runaway propagation and, therefore, the need to include combustion calculations in simulation models. A simulation model without combustion incorrectly predicts no thermal runaway propagation, whereas, when combustion is modeled, it is found that thermal runaway propagation indeed occurs.

Effect of location of vent hole.—It is of much interest to understand how the location of the vent hole influences the propagation of thermal runaway. In general, vent gases may eject out of a hole on the top surface of the cell when the pressure in the

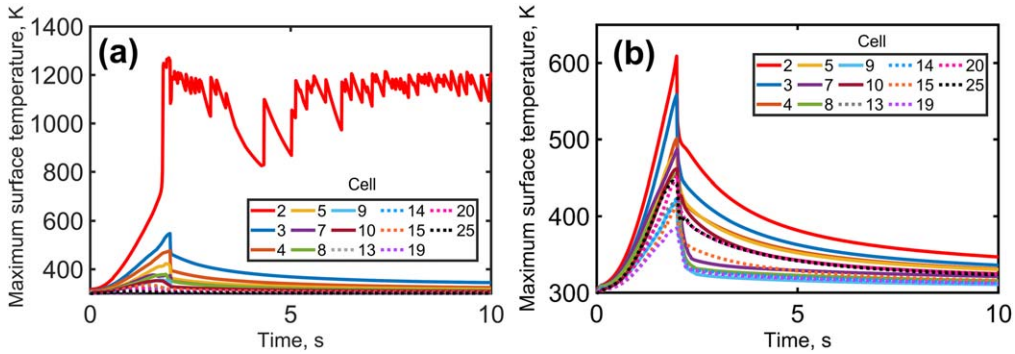

Figure 7. Impact of combustion modeling: Temperature plots for the case of 2 s venting from a 7 mm^2 vent placed at center of top surface of cell 1. (a) and (b) present results for cases in which venting and combustion are both modeled, and in which, only venting is modeled, respectively. In both cases, overhead gap and cell-cell gap are 5 mm and 4 mm, respectively.

cell rises too much and the relief valve located on the top cap opens to release the vent gases. On the other hand, excessive pressure is the cell may also cause rupture in the cell body, causing rupture and ejection from the weakest point, which may be located anywhere on the cell body.[48] Given the uncertainty of the location of failure, it is of interest to understand how differently the thermal runaway propagation process may occur in these cases. Two particular cases are considered here—in the first case, a 7 mm^2 vent hole is located at the center of the top surface of the trigger cell. In the second case, a vent hole of the same size is located on the curved surface of the trigger cell, 2.5 mm below the top end and directly facing cell 2. All other problem parameters in the two cases are the same as each other, corresponding to the parameters used in Fig. 2. Figure 8 plots temperature curves for various cells for the second case in which the vent hole is located on the curved surface. For comparison, temperature curves for the baseline case are presented in Fig. 7a. These plots clearly show that when the vent hole is located on the top surface of the cell, thermal runaway propagation occurs only to cell 2, while other cells do not undergo thermal runaway despite getting hotter. This may be attributed to the upwards pointing vent hole, due to which, vent gases exit upwards, and the combustion

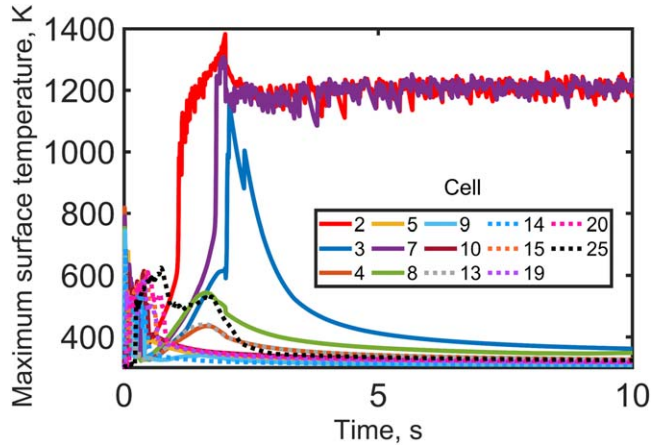

Figure 8. Effect of location of vent: Temperature plots for 1 mm overhead and cell-to-cell gap, 2 s venting time and 7 mm^2 vent placed at 62.5 mm height on curved surface of trigger cell directly facing cell 2. For comparison, temperature plots for the baseline case are presented in Fig. 7a.

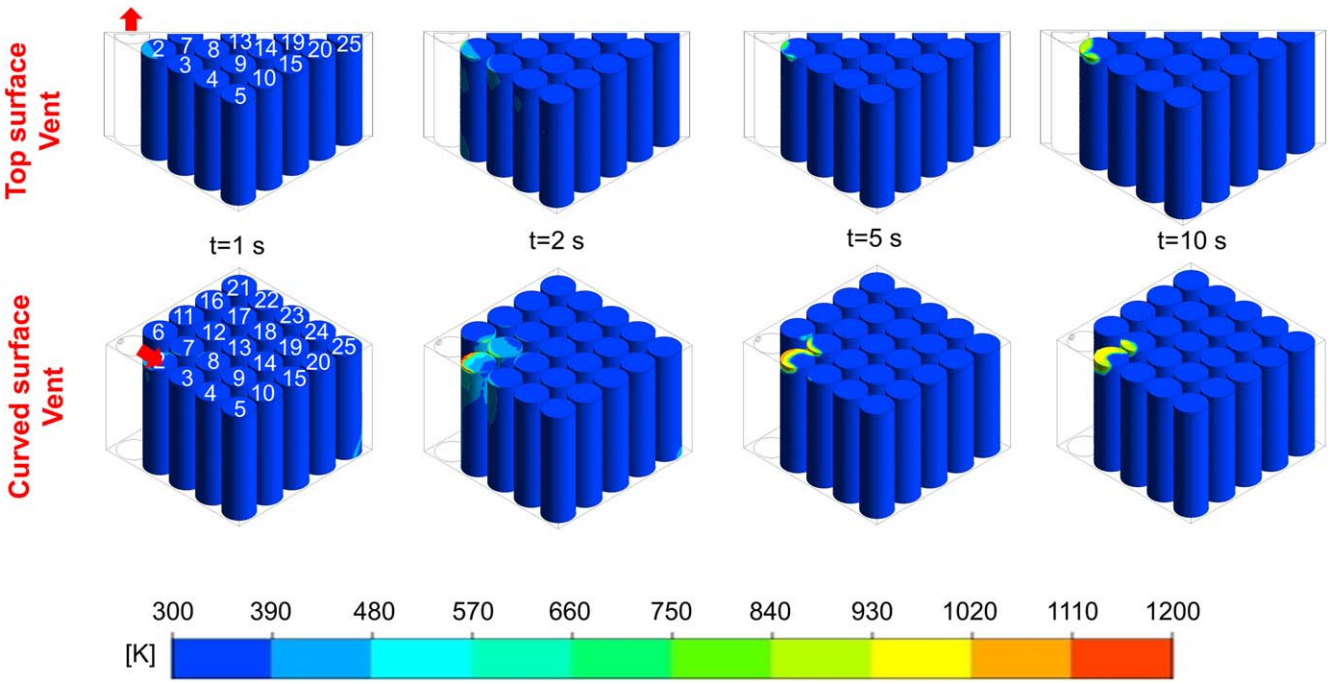

Figure 9. Colorplots at different timesteps for the two vent locations presented in Fig. 8.

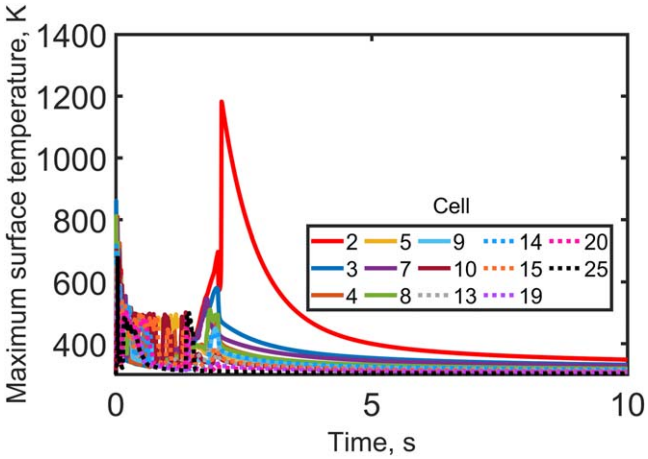

Figure 10. Impact of speed of vent gases: Temperature plots for the case of 2 s venting from a 7 mm^2 vent placed at center of top surface of cell 1, with twice the vent speed compared to the baseline case presented in Fig. 7a. Overhead gap and cell-cell gap are 5 mm and 4 mm, respectively.

process occurs above the trigger cell, thereby having a limited impact on other cells. On the other hand, when the vent hole is located on the curved surface facing cell 2, combustion occurs in the thin space between the cells, which particularly impacts cells 2 and 7 –the two cells that are closest to the trigger cell. As Fig. 8 shows, thermal runaway propagates to both cells 2 and 7 in this case. This clearly highlights the distinction in thermal runaway propagation depending on the location and direction of the venting event. For further illustration and comparison, temperature contour plots for the two cases are presented at different times in Fig. 9. These plots show spreading of thermal runaway to only cell 2 when the vent hole is located at the top of the trigger cell, and to both cells 2 and 7 when the vent hole is located on the side wall. Note that in this work, secondary thermal runaway propagation is not accounted for. Once the neighboring cells enter thermal runaway and combustion of gases venting from neighboring cells occurs, it is quite likely that, based on the results from this work, further outwards propagation of thermal runaway will occur.

Effect of the venting speed.—Additional simulations are carried out to understand the effect of venting speed on thermal runaway propagation. The venting gas velocity can impose complex nonlinear effects on flow, mixing, combustion and heat transfer, which eventually can substantially and non-intuitively alter the results of thermal runaway propagation. For example, slight increase in venting speed can enhance mixing, and promote turbulent flame propagation by increasing the flame surface area through corrugations and wrinkles, which will largely promote venting gas combustion induced thermal runaway. On the other hand, increased venting speed can reduce local residence time for combustion reaction and heat transfer to the battery. The baseline simulation reported in Fig. 7a is compared with a new simulation with double the inlet velocity. As shown in Fig. 10 for this case, it is found that doubling the inlet velocity actually suppresses thermal runaway propagation. The maximum battery surface temperature during the venting period also exhibits a large fluctuation from increased turbulent intensity. The suppression of thermal runaway propagation at larger inlet speed is confirmed from OH concentration plots for this case shown in Fig. 11, which show much faster spread of the reaction fronts due to stronger turbulence compared to the baseline case shown in Fig. 5b. Eventually, due to the reduced residence time of reaction front propagation, heat transfer to the immediately adjacent cell 2 is substantially reduced, and consequently, no self-sustained thermal runaway is initiated. Meanwhile, it is seen that the flame with increased venting speed heats up many cells by a large extent along its path, including almost every cell in the early venting stages and as far as cells 14 and 15 in the later stages, but does not effectively heat up any of them to the threshold condition of thermal runaway. This result suggests the important role of venting speed on thermal

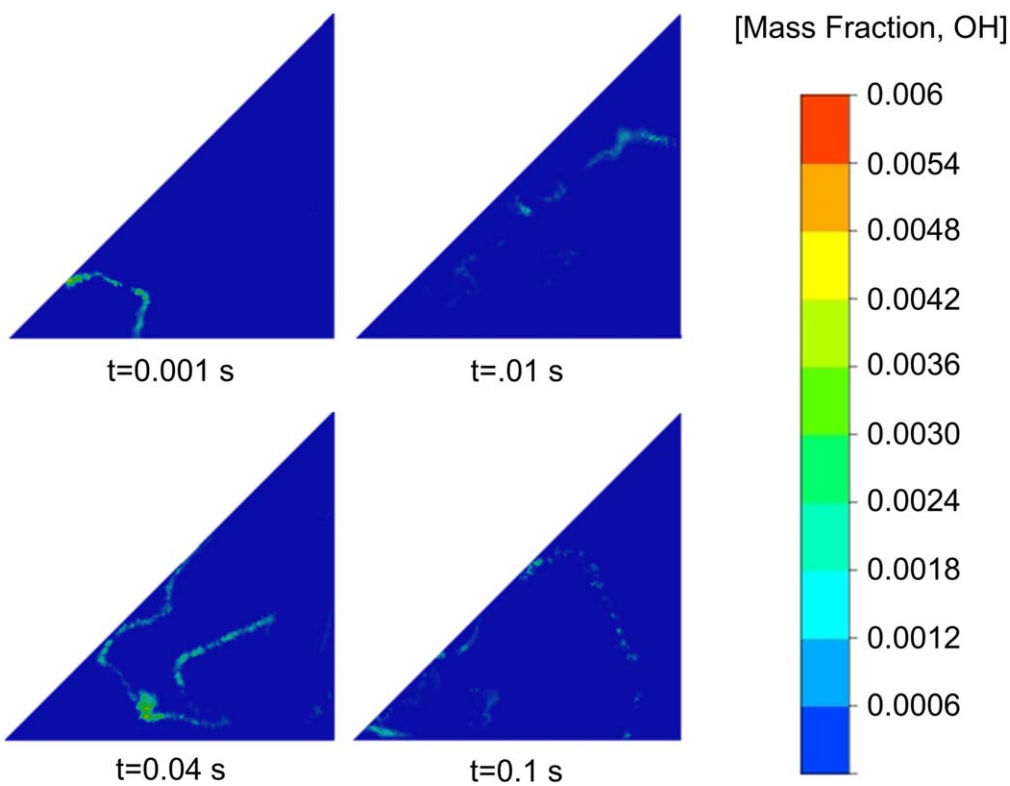

Figure 11. Impact of speed of vent gases: OH concentration colorplots at multiple times on an XY cross-section plane 1 mm above the top end of cells. Problem parameters correspond to Fig. 10.

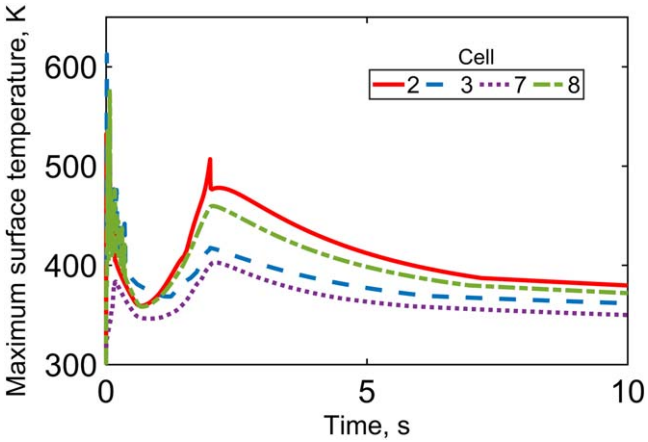

Figure 12. Impact of location of trigger cell: Temperature plots for the case of 2 s venting from a 7 mm^2 vent placed at center of top surface of the cell at the center of the pack (cell 13). All other parameters are the same as the baseline simulation.

runaway propagation. Due to non-linear effects involved in turbulent combustion, a systematic, mathematical study of these processes merits future efforts.

Effect of location of trigger cell.—All simulations discussed so far are based on the trigger cell at the corner of the battery pack (i.e., cell 1). Another simulation is carried out to investigate the effect of location of the trigger cell. In particular, the case of the trigger cell at the center of the battery pack (i.e., cell 13) is considered. Temperature plots for this case are presented in Fig. 12, and may be compared with the plots for the baseline case of trigger cell at the corner shown in Fig. 7a. Considering the significant symmetry that exists when cell 13 is the trigger cell, temperature plots for only a few cells in the vicinity of the trigger cell are presented. Figure 12 shows that in this case, even though the neighboring cells heat up somewhat, there is no sustained propagation of thermal runaway. This is because compared to the baseline case of the trigger cell 1 at the corner, where the wall redirects a large portion of the ejecta back to cell 2 and triggers thermal runaway, there are more neighboring cells around the center cell 13, such that the ejecta and the heat due to combustion is spread out and more evenly distributed in all radial directions. This consequently weakens the overall impact of hot combustion products on each neighboring cell. Due to such a wider distribution of the combustion-related thermal energy, there is no propagation of thermal runaway when the trigger cell is at the center. This comparison demonstrates the key role played by the location of the trigger cell on thermal runaway propagation in the battery pack, and the capability of the present simulations to account for such geometrical effects.

Conclusions

The key contribution of this work is in comprehensive modeling of combustion of vent gases during thermal runaway and the subsequent impact on thermal runaway propagation. This modeling has been carried out within a comprehensive simulations framework that accounts for multiple other non-linear phenomena such as Arrhenius heat generation, radiation and turbulent mixing. Good agreement with experimental data for a test case provides validation of the simulation approach, based on which, it is shown that combustion of vent gases is a very important process to model in studying thermal runaway propagation.

It is important to note the key limitations and assumptions inherent in this work. The Reynolds-averaged Navier–Stokes (RANS) based turbulent combustion modeling cannot accurately resolve the fine reaction zone and turbulent-chemistry interaction at small length scales. In the meantime, the boundary layer at the surface of the battery can strongly affect the heat transfer process, and its separation can lead to more complexity in the flow field. Therefore, an ideal simulation would be Direct Numerical Simulation (DNS) that fully resolves flow, mixing, chemistry, heat transfer and thermal runaway. This is, however, very chalenging due to the substantial computational resources needed.

This work expands the fundamental understanding of combustion during thermal runaway in a Li-ion battery pack, particularly the impact of combustion on thermal runaway propagation. In addition to these fundamental insights, the results presented here are also of considerable practical importance in the thermal design and optimization of battery packs, towards preventing thermal runaway propagation. It is expected that guidelines based on this work may help improve the safety and performance of electrochemical energy conversion and storage systems.

Acknowledgments

This material is based upon work supported by CAREER Award No. CBET-1554183 from the National Science Foundation.

ORCID

Peng Zhao https://orcid.org/0000-0002-6743-6269
Ankur Jain https://orcid.org/0000-0001-5573-0674

References

1. K. Shah, V. Vishwakarma, and A. Jain, "Measurement of multiscale thermal transport phenomena in Li-ion cells: a review." *J Electrochem Energy Convers Storage.*, **13**, 030801 (2016).
2. T. M. Bandhauer, S. Garimella, and T. F. Fuller, "A critical review of thermal issues in Lithium-ion batteries." *J. Electrochem. Soc.*, **158**, R1 (2011).
3. R. Spotnitz and J. Franklin, "Abuse behavior of high-power, lithium-ion cells." *J. Power Sources*, **113**, 81 (2003).
4. A. Melcher, C. Ziebert, M. Rohde, and H. J. Seifert, "Modeling and simulation of the thermal runaway behavior of cylindrical Li-ion cells-computing of critical parameters." *Energies.*, **9**, 1 (2016).
5. P. T. Coman, S. Mátéfi-Tempfli, C. T. Veje, and R. E. White, "Modeling vaporization, gas generation and venting in Li-ion battery cells with a dimethyl carbonate electrolyte." *J. Electrochem. Soc.*, **164**, A1858 (2017).
6. P. Jindal and J. Bhattacharya, "Review—understanding the thermal runaway behavior of Li-ion batteries through experimental techniques." *J. Electrochem. Soc.*, **166**, A2165 (2019).
7. A. W. Golubkov, D. Fuchs, J. Wagner, H. Wiltsche, C. Stangl, G. Fauler, G. Voitic, A. Thler, and V. Hacker, "Thermal-runaway experiments on consumer Li-ion batteries with metal-oxide and olivin-type cathodes." *RSC Adv.*, **4**, 3633 (2014).
8. X. Feng et al., "Investigating the thermal runaway mechanisms of lithium-ion batteries based on thermal analysis database." *Appl. Energy*, **246**, 53 (2019).
9. S. Abada, M. Petit, A. Lecocq, G. Marlair, V. Sauvant-Moynot, and F. Huet, "Combined experimental and modeling approaches of the thermal runaway of fresh and aged lithium-ion batteries." *J. Power Sources*, **399**, 264 (2018).
10. A. O. Said, C. Lee, S. I. Stoliarov, and A. W. Marshall, "Comprehensive analysis of dynamics and hazards associated with cascading failure in 18650 lithium ion cell arrays." *Appl. Energy*, **248**, 415 (2019).
11. C. F. Lopez, J. A. Jeevarajan, and P. P. Mukherjee, "Evaluation of combined active and passive thermal management strategies for lithium-ion batteries." *J Electrochem Energy Convers Storage.*, **13**, 031007 (2016).
12. C. Jin et al., "Model and experiments to investigate thermal runaway characterization of lithium-ion batteries induced by external heating method." *J. Power Sources*, **504**, 230065 (2021).
13. Z. Huang, C. Zhao, H. Li, W. Peng, Z. Zhang, and Q. Wang, "Experimental study on thermal runaway and its propagation in the large format Lithium ion battery module with two electrical connection modes." *Energy*, **205**, 117906 (2020).
14. Z. Huang, X. Li, Q. Wang, Q. Duan, Y. Li, L. Li, and Q. Wang, "Experimental investigation on thermal runaway propagation of large format lithium ion battery modules with two cathodes." *Int J Heat Mass Transf.*, **172**, 121077 (2021).
15. X. Feng, J. Sun, M. Ouyang, F. Wang, X. He, L. Lu, and H. Peng, "Characterization of penetration induced thermal runaway propagation process within a large format lithium ion battery module." *J. Power Sources*, **275**, 261 (2015).
16. K. Shah, D. Chalise, and A. Jain, "Experimental and theoretical analysis of a method to predict thermal runaway in Li-ion cells." *J. Power Sources*, **330**, 167 (2016).
17. D. Ren, X. Liu, X. Feng, L. Lu, M. Ouyang, J. Li, and X. He, "Model-based thermal runaway prediction of lithium-ion batteries from kinetics analysis of cell components." *Appl. Energy*, **228**, 633 (2018).
18. M. Parhizi, M. B. Ahmed, and A. Jain, "Determination of the core temperature of a Li-ion cell during thermal runaway." *J. Power Sources*, **370**, 27 (2017).
19. L. Zhang, P. Zhao, M. Xu, and X. Wang, "Computational identification of the safety regime of Li-ion battery thermal runaway." *Appl. Energy*, **261**, 114440 (2020).

20. X. Feng, L. Lu, M. Ouyang, J. Li, and X. He, "A 3D thermal runaway propagation model for a large format lithium ion battery module." *Energy*, **115**, 194 (2016).
21. D. Mishra and A. Jain, "Multi-mode heat transfer simulations of the onset and propagation of thermal runaway in a pack of cylindrical li-ion cells." *J. Electrochem. Soc.*, **168**, 20504 (2021).
22. T. D. Hatchard, D. D. MacNeil, D. A. Stevens, L. Christensen, and J. Dahn, "Importance of heat transfer by radiation in Li-ion batteries during thermal abuse." *Electrochem. Solid-State Lett.*, **3**, 305 (2000).
23. D. Mishra, K. Shah, and A. Jain, "Investigation of the impact of radiative shielding by internal partitions walls on propagation of thermal runaway in a matrix of cylindrical li-ion cells." *J. Electrochem. Soc.*, **168**, 120507 (2021).
24. H. Zhai, H. Li, P. Ping, Z. Huang, and Q. Wang, "An experimental-based domino prediction model of thermal runaway propagation in 18,650 lithium-ion battery modules." *Int J Heat Mass Transf.*, **181**, 122024 (2021).
25. J. K. Ostanek, W. Li, P. P. Mukherjee, K. R. Crompton, and C. Hacker, "Simulating onset and evolution of thermal runaway in Li-ion cells using a coupled thermal and venting model." *Appl. Energy*, **268**, 114972 (2020).
26. P. T. Coman, S. Rayman, and R. E. White, "A lumped model of venting during thermal runaway in a cylindrical Lithium Cobalt Oxide lithium-ion cell." *J. Power Sources*, **307**, 56 (2016).
27. D. Mishra, K. Shah, and A. Jain, "Investigation of the impact of flow of vented gas on propagation of thermal runaway in a li-ion battery pack." *J. Electrochem. Soc.*, **168**, 060555 (2021).
28. D. Kong, G. Wang, P. Ping, and J. Wen, "A coupled conjugate heat transfer and CFD model for the thermal runaway evolution and jet fire of 18650 lithium-ion battery under thermal abuse." *eTransportation.*, **12**, 100157 (2022).
29. P. Ribière, S. Grugeon, M. Morcrette, S. Boyanov, S. Laruelle, and G. Marlair, "Investigation on the fire-induced hazards of Li-ion battery cells by fire calorimetry." *Energy Environ. Sci.*, **5**, 5271 (2012).
30. F. Larsson, P. Andersson, and B. E. Mellander, "Lithium-ion battery aspects on fires in electrified vehicles on the basis of experimental abuse tests." *Batteries.*, **2**, 1 (2016).
31. A. Lecocq, G. G. Eshetu, S. Grugeon, N. Martin, S. Laruelle, and G. Marlair, "Scenario-based prediction of Li-ion batteries fire-induced toxicity." *J. Power Sources*, **316**, 197 (2016).
32. G. G. Eshetu, J. P. Bertrand, A. Lecocq, S. Grugeon, S. Laruelle, M. Armand, and G. MArlair, "Fire behavior of carbonates-based electrolytes used in Li-ion rechargeable batteries with a focus on the role of the LiPF6 and LiFSI salts." *J. Power Sources*, **269**, 804 (2014).
33. J. Xu, P. Guo, Q. Duan, X. Yu, L. Zhang, Y. Liu, and Q. Wang, "Experimental study of the effectiveness of three kinds of extinguishing agents on suppressing lithium-ion battery fires." *Appl. Therm. Eng.*, **171**, 115076 (2020).
34. Y. Liu, Q. Duan, J. Xu, H. Li, J. Sun, and Q. Wang, "Experimental study on a novel safety strategy of lithium-ion battery integrating fire suppression and rapid cooling." *J Energy Storage.*, **28**, 101185 (2020).
35. M. Chen, R. Yuen, and J. Wang, "An experimental study about the effect of arrangement on the fire behaviors of lithium-ion batteries." *J. Therm. Anal. Calorim.*, **129**, 181 (2017).
36. C. M. R. Vendra, A. V. Shelke, J. E. H. Buston, J. Gill, D. Howard, E. Read, A. Abaza, B. Cooper, and J. X. Wen, "Numerical and experimental characterisation of high energy density 21700 lithium-ion battery fires." *Process Saf. Environ. Prot.*, **160**, 153 (2022).
37. Y. Takagishi, Y. Tozuka, T. Yamanaka, and T. Yamaue, "Heating simulation of a Li-ion battery cylindrical cell and module with consideration of gas ejection." *Energy Reports.*, **8**, 3176 (2022).
38. F. A. Mier, M. J. Hargather, and S. Ferreira, "Experimental quantification of vent mechanism flow parameters in 18650 format lithium ion batteries." *J Fluids Eng Trans ASME.*, **141**, 1 (2019).
39. F. A. Williams, *Combustion Theory.* (Boca Raton, FL)(CRC Press) (2018).
40. Z. Luo, C. S. Yoo, E. S. Richardson, J. H. Chen, C. K. Law, and T. Lu, "Chemical explosive mode analysis for a turbulent lifted ethylene jet flame in highly-heated coflow." *Combust. Flame*, **159**, 265 (2012).
41. Z. Yang and T. H. Shih, *AIAAJ*, **31**, 11752 (2012) .
42. S. J. Drake, D. A. Wetz, J. K. Ostanek, S. P. Miller, J. M. Heinzel, and A. Jain, "Measurement of anisotropic thermophysical properties of cylindrical Li-ion cells." *J. Power Sources*, **252**, 298 (2014).
43. I. H. Bell, S. Quoilin, J. Wronski, and V. Lemort, "Coolprop: an open-source reference-quality thermophysical property library." *ASME ORC 2nd International Seminar on ORC Power Systems.* (2013).
44. A. W. Golubkov, S. Scheikl, R. Planteu, G. Voitic, H. Wiltsche, C. Stangl, G. Fauler, A. Thaler, and V. Hacker, "Thermal runaway of commercial 18650 Li-ion batteries with LFP and NCA cathodes - impact of state of charge and overcharge." *RSC Adv.*, **5**, 57171 (2015).
45. W. Meier, R. S. Barlow, Y. L. Chen, and J. Y. Chen, "Raman/Rayleigh/LIF measurements in a turbulent CH_4/H2/N2 jet diffusion flame: experimental techniques and turbulence-chemistry interaction." *Combust. Flame*, **123**, 326 (2000).
46. H. Wang, "Consistent flamelet modeling of differential molecular diffusion for turbulent non-premixed flames." *Phys. Fluids*, **28**, 035102 (2016).
47. A. K. Chatzopoulos and S. Rigopoulos, "A chemistry tabulation approach via rate-controlled constrained equilibrium (RCCE) and artificial neural networks (ANNs), with application to turbulent non-premixed CH_4/H2/N2 flames." *Proc. Combust. Inst.*, **34**, 1465 (2013).
48. J. Kim, A. Mallarapu, D. P. Finegan, and S. Santhanagopalan, "Modeling cell venting and gas-phase reactions in 18650 lithium ion batteries during thermal runaway." *J. Power Sources*, **489**, 229496 (2021).